

# Doping-Induced Spectral Shifts in Two Dimensional Metal Oxides

E. R. YLVIKAKER AND W. E. PICKETT

*Department of Physics, University of California Davis, Davis, California 95616*

PACS 74.10.+v – Occurrence, potential candidates

PACS 74.20.Pq – Electronic structure calculations

PACS 74.72.-h – Cuprate superconductors

**Abstract.** - Doping of strongly layered ionic oxides is an established paradigm for creating novel electronic behavior. This is nowhere more apparent than in superconductivity, where doping gives rise to high temperature superconductivity in cuprates (hole-doped) and to surprisingly high  $T_c$  in HfNCl ( $T_c=25.5\text{K}$ , electron-doped). First principles calculations of hole-doping of the layered delafossite  $\text{CuAlO}_2$  reveal unexpectedly large doping-induced shifts in spectral density, strongly in opposition to the rigid band picture that is widely used as an accepted guideline. These spectral shifts, of similar origin as the charge transfer used to produce negative electron affinity surfaces, drastically alter the character of the Fermi level carriers, leading in this material to an O-Cu-O molecule-based carrier rather than a nearly pure-Cu hole as in a rigid band picture. First principles linear response electron-phonon coupling (EPC) calculations reveal, as a consequence, net *weak EPC* and no superconductivity rather than the high  $T_c$  obtained previously using the rigid band expectation. These specifically two-dimensional dipole-layer driven spectral shifts provides new insights into materials design in layered materials.

The quest for new materials functionalities is especially vigorous in transition metal oxides (TMOs), with quasi-two dimensional (q2D) classes causing great activity. The cuprate superconductors, with high superconducting critical temperature (HTS)  $T_c$ , provide the most prominent example, but doping-induced superconductivity arises in numerous other unexpected systems:  $\text{MnCl}$ ,  $\mathcal{M} = \text{Ti, Zr, Hf}$  ( $T_c=15\text{-}25\text{K}$ );  $\text{MgB}_2$ , a self-hole-doped superconductor at  $40\text{K}$ ; the triangular lattice oxides  $\text{Li}_x\text{NbO}_2$ ,  $\text{Na}_x\text{CoO}_2$ , and chalcogenides  $\text{Cu}_x\text{TiSeO}_2$  and  $\text{A}_x\mathcal{T}\text{S}_2$  ( $\text{A}=\text{alkali}$ ,  $\mathcal{T}=\text{transition metal}$ ), all with [1]  $T_c \sim 5\text{K}$ . The cuprates, followed by  $\text{MgB}_2$  and then by the Fe pnictide superconductors (FeSCs) with  $T_c$  up to  $56\text{K}$ , have illustrated that excellent superconductors appear in surprising regions of the materials palette. Even the FeSCs can be pictured as doped (or self-doped) semimetallic superconductors.

The  $\text{CuO}_2$  square-lattice cuprates have inspired study – the computational design – of related square-lattice transition metal oxides, such as the “charge conjugate” vanadate [2–4]  $\text{Sr}_2\text{VO}_4$ , the  $\text{Ag}^{2+}$  material [5]  $\text{Cs}_2\text{AgF}_4$  that is isostructural and isovalent with  $\text{La}_2\text{CuO}_4$ , and cuprate-spoofing artificially layered nickelates, [6] so far without finding new superconductors. [7, 8] These highly interesting materials, though unfruitful for their original intent, suggests that a more detailed understanding of doping effects is necessary to unravel

the mechanism of pairing in q2D systems. Nevertheless, materials property design can and does proceed when there is some broad understanding of the mechanism underlying the property. [9–13]

The superconducting pairing mechanism is only well understood for electron-phonon coupling (EPC) where  $\text{MgB}_2$  with  $T_c=40\text{K}$  is most successful so far. The detailed understanding of EPC through strong-coupling Eliashberg theory [14] encourages rational, specific optimization of the EPC strength  $\lambda$  and of  $T_c$ , and specific guidelines for one direction for increasing  $T_c$  have been laid out. [15]

Recently a new and different class of cuprate, the delafossite structure  $\text{CuAlO}_2 \equiv \text{AlCuO}_2$ , has been predicted by Nakanishi and Katayama-Yoshida [16] (NK) to be a  $T_c \approx 50\text{K}$  superconductor when sufficiently hole doped. The calculated EPC strength and character is reminiscent of that of  $\text{MgB}_2$ , whose high  $T_c$  derives from a specific mode (O-Cu-O stretch for  $\text{CuAlO}_2$ ) and focusing in  $q$ -space [17–20] due to the circular shape of the quasi-two dimensional (2D) Fermi surface (FS).  $\text{CuAlO}_2$  is another layered cuprate, with Cu being (twofold) coordinated by O ions in a layered crystal structure. The differences with square-lattice cuprates are however considerable: the Cu sublattice is not square but triangular; there are *only* apical oxygen neighbors; the undoped compound is a  $d^{10}$  band insulator rather than a  $d^9$  antiferromagnetic Mott insulator; it

is nonmagnetic even when lightly doped; and it is most heavily studied as a *p*-type transparent conductor. [21] It shares with the hexagonal  $\mathcal{MNCl}$  system that doped-in carriers enter at a *d* band edge. NK provided computational evidence for impressively large  $\lambda$  and high temperature superconductivity  $T_c$  up to 50 K when this compound is hole-doped, *viz.*  $\text{CuAl}_{1-x}\text{Mg}_x\text{O}_2$ . It is known that the delafossite structure is retained at least to  $x=0.05$  upon coping with Mg. [22] If this prediction could be substantiated, a new and distinctive structural class would be opened up for a more concerted search for high temperature superconductors (HTS).

When our initial linear response calculations indicated weak (rather than strong) EPC, we performed a more comprehensive study. In their work, NK did not carry out linear response calculations of electron-phonon coupling for doped  $\text{CuAlO}_2$ . Instead they made the reasonable-looking simplifications of (a) calculating phonons and EP matrix elements for the undoped insulator, (b) moving the Fermi level in a rigid-band fashion, and (c) using those quantities to evaluate *q*-dependent coupling ( $\lambda_q$ ; *q* includes the branch index) and finally  $\lambda$ , predicting  $T_c$  up to 50K. In this paper we provide the resolution to this discrepancy, which involves the crucial effect of large doping-induced spectral weight redistribution due to non-rigid-band shifts of spectral density upon doping. The interlayer charge transfer underlying the shift in spectral density has the same origin as the charge transfer obtained from alkali atom adlayers on oxygenated [23] and native [24] diamond surfaces to produce negative electronic affinity structures. This “mechanism” of electronic structure modification will be useful in designing materials for functionalities other than superconductivity. The spectral shifts are distinct from those discussed in the doping of a Mott insulator as we discuss below.

First principles electronic structure calculations were performed within density functional theory (DFT) using the FPLO code [25] to obtain the electronic structure for both undoped and doped materials, the latter one being carried out in the virtual crystal approximation (VCA), where the (say)  $\text{Al}_{1-x}\text{Mg}_x$  sublattice (Ca substitution is also an option) that gives up its valence electrons is replaced by an atom with an averaged nuclear charge. VCA allows charge transfer to be obtained self-consistently, neglecting only disorder in the Al-Mg layer. The result is the transfer of *x* electrons per f.u. from Cu, with half going to each of the neighboring Al-Mg layers, corresponding to metallic Cu  $d^{10-x}$ . Phonon spectra and electron-phonon coupling calculations for the doped system were performed using ABINIT [26] version 6.6.3 with norm-conserving Trouiller-Martins pseudopotentials. In both codes the Perdew-Wang 92 GGA (generalized gradient approximation) functional [27] was used. The phonon and EPC calculations were done on the rhombohedral unit cell using a  $24^3$  k-point mesh and an  $8^3$  q-point mesh, interpolated to more q-points.

The measured structural parameters [28] for  $\text{CuAlO}_2$  used were for rhombohedral  $R\bar{3}m$  (#166) structure with  $a = 5.927$  Å,  $\alpha = 27.932^\circ$ . This structure is equivalent to  $a = 2.861$  Å,  $c = 17.077$  Å with hexagonal axes. Cu resides on the  $1a$  site

at the origin, Al is at the  $1b$  site, at  $(\frac{1}{2}, \frac{1}{2}, \frac{1}{2})$  and the O atom is in the  $2c$  position  $(u, u, u)$ ,  $u = 0.1101$ .

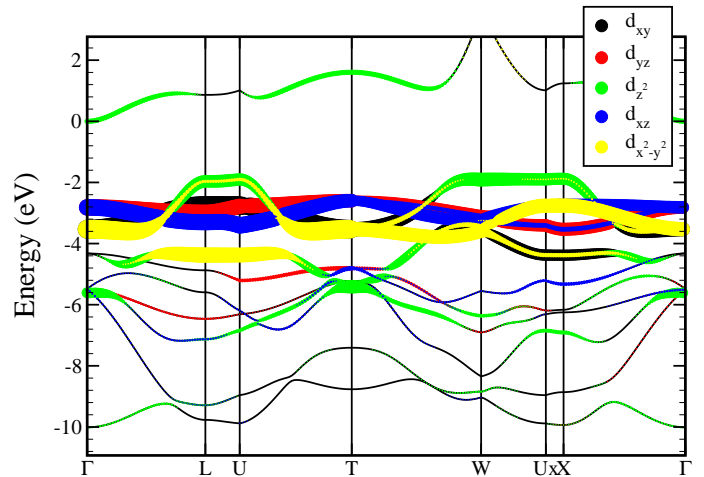


Fig. 1: (color online) Fatbands plot for  $\text{CuAlO}_2$ , with zero of energy at the top of the gap. The size of the symbol represents the amount of  $3d$  character, and the color the character as given in the legend.

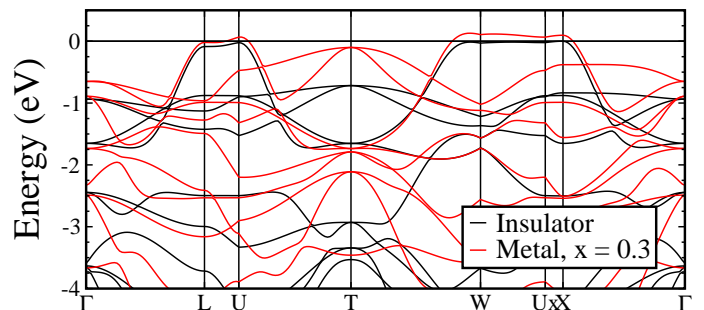


Fig. 2: (color online) Comparison of band structures for the metallic and insulating states of  $\text{CuAl}_{1-x}\text{Mg}_x\text{O}_2$  with  $x = 0.3$ . This moderate level of doping results in very strong changes in the relative band positions.

The band structure of insulating  $\text{CuAlO}_2$  shown in Fig. 1, which agrees with previous work, [16, 29, 30] illustrates that Cu  $3d$  bands form a narrow, 2.5 eV wide complex at the top of the valence bands. Oxygen  $2p$  bands occupy the region -8 eV to -3 eV below the gap. This compound is a closed shell  $\text{Cu}^+\text{Al}^{3+}(\text{O}^{2-})_2$  ionic insulator with minor metal-O covalence, although enough to stabilize this relatively unusual, strongly layered structure.

The upper valence bands providing the hole states consist of  $d_{z^2}$  character with some in-plane  $d_{xy}$ ,  $d_{x^2-y^2}$  mixing. The top of this band occurs at the edge of Brillouin zone (BZ) as in, for example, graphene, but it is anomalously flat along the edge of the zone, *viz.*  $Ux$ - $W$  (M-K, in hexagonal notation), which comprises the entire edge of the BZ. Since it is also almost dispersionless in the  $\hat{z}$  direction, the resulting density of states just below the gap reflects a *one-dimensional phase space*, as shown in Fig. 3a. The  $d_{xy}$ ,  $d_{x^2-y^2}$  bands are nearly flat in

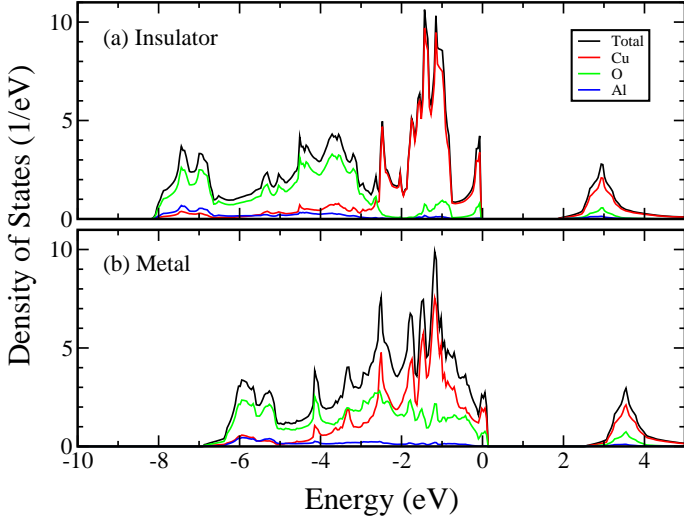


Fig. 3: (color online) Comparison of the density of states for the (a) insulating  $\text{CuAlO}_2$  and (b) metallic  $\text{CuAl}_{1-x}\text{Mg}_x\text{O}_2$  with  $x = 0.3$ . For the insulator, the Cu  $d$  bands are rather separate from the O  $p$  bands, but upon doping strong O  $p$  permeates the Cu  $d$  bands, to near the Fermi level.

the -2 to -1 eV region, and the  $d_{xz}, d_{yz}$  bands are even flatter, at -1 to -0.5 eV. These four flat bands reflect very minor  $d$ - $d$  hopping in the plane.

When hole-doped, a dramatic shift of spectral weight occurs in the occupied bands, as is evident in both Figs. 2 for the bands and 3 for the spectral density. With the top (Cu  $d_{z^2}$ ) conduction band as reference, the  $3d$ - $2p$  band complex at all lower energies readjusts rapidly with doping to lower binding energies. The  $d_{xz}, d_{yz}$  bands (Fig. 1) acquire considerable  $2p$  character and move up to nearly touch  $E_F$  at the point  $\Gamma=(0,0,\pi/c)$ ; further doping will introduce holes into this band. The O  $2p$  bands, which lay below the  $3d$  bands in the insulator, have shifted upward dramatically by 2 eV (a remarkably large 70 meV/% doping), contributing extra screening at and near  $E_F$  in the metallic phase. The gap increases by  $\sim 0.5$  eV. These spectral shifts can be accounted for by a charge-dipole layer potential shift due to the  $\text{Cu} \rightarrow \text{Al-Mg}$  layer charge transfer. The increased  $3d - 2p$  hybridization is made more apparent in Fig. 4, which reveals that the  $d_{xz}, d_{yz}$  bands at  $\Gamma$  (and elsewhere) have increased contribution from the O  $p$  states. Also apparent in this plot are seemingly extra bands appearing at about -1 eV near  $\Gamma$ ; these are bands from below which have been shifted strongly upward by  $\sim 2$  eV by the dipole potential shift resulting from charge transfer.

More light is shed on the electronic structure of  $\text{CuAl}_{1-x}\text{Mg}_x\text{O}_2$  by using Wannier functions (WFs) to construct a tight binding model of the states near the Fermi level. We use the WF generator in the FPLO code. [25] These WFs are symmetry respecting atom-based functions, [31] constructed by projecting Kohn-Sham states onto, in this case, the Cu  $3d_{z^2}, 3d_{xy}, 3d_{x^2-y^2}$  atomic orbitals, with resulting hopping amplitudes shown in Table 1. Hoppings involving the  $xy$  and

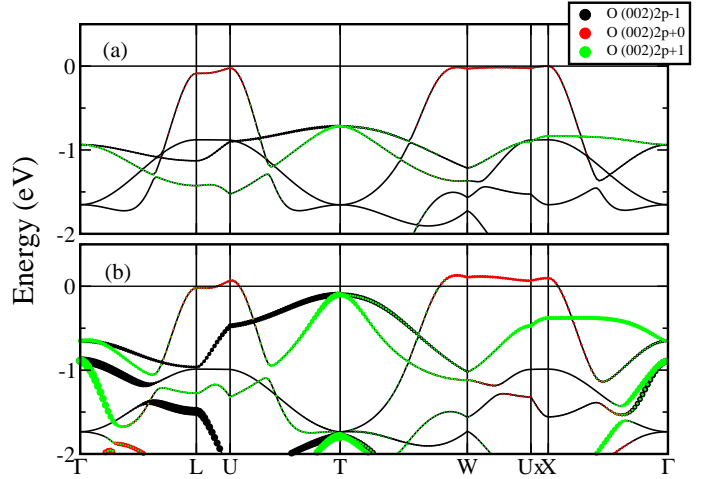


Fig. 4: (color online) Fatband plots for the (a) insulator and (b)  $x=0.3$  metal states, emphasizing O  $2p$  character. In addition to the strong shift upward, the O  $2p$  character has increased many-fold for the bands near  $E_F$  in the metal.

$x^2 - y^2$  orbitals are not significantly different between the insulator and metal. However, hopping amplitudes for the  $d_{z^2}$  WF change significantly, the most important being the factor of 2.5 increase in the *hopping between layers*,  $t_{\perp}$ . Consistent with the picture from the DOS, the hoppings for the metallic state are more long-range: nearest neighbor hopping drops by 13%, while third neighbor hopping nearly doubles. All of these changes are neglected in a rigid band treatment.

This band dispersion is anomalous for a quasi-2D structure such as this, where normally the  $3d$  orbitals with lobes extending in the  $x - y$  plane would be expected to be the most dispersive. Instead, it is the  $d_{z^2}$  band that disperses, with a bandwidth of 2.5 eV and the band bottom at  $\Gamma$ . Shown in Fig. 5 is the  $d_{z^2}$ -projected WF for the  $x=0.3$  hole-doped metal. Consistent with their minor dispersion, the WFs for the other  $3d$  orbitals (not shown) have little contribution beyond the atomic orbital, showing only minor anti-bonding contributions from nearby O atoms.

The  $d_{z^2}$  WF shape is, in addition, quite extraordinary. Although displaying  $d_{z^2}$  symmetry as it must, its shape differs strikingly from atomic form. It is so much fatter in the  $x$ - $y$  plane than the bare  $d_{z^2}$  orbital that it is difficult to see the signature  $m_{\ell} = 0$  “ $z^2$ ” lobes pictured in textbooks. This shape is due, we think, to “pressure” from the neighboring antibonding O  $p_z$  orbitals above and below. There is an (expected) admixture of O  $2p_z$  orbitals, as well as a small symmetry-allowed  $p_z + (p_x, p_y)$  contribution from the neighboring oxygen ions that finally provides (with their overlap) the in-plane dispersion of the  $d_{z^2}$  band. The important qualitative difference compared to the insulator WF is the contribution from O atoms in the *next nearest* planes (across the Al layer) whose states have been shifted upward by the doping-induced charge transfer. This mixing opens a channel for hopping between layers in the Cu  $d_{z^2}$  WFs by creating overlap in the two planes of

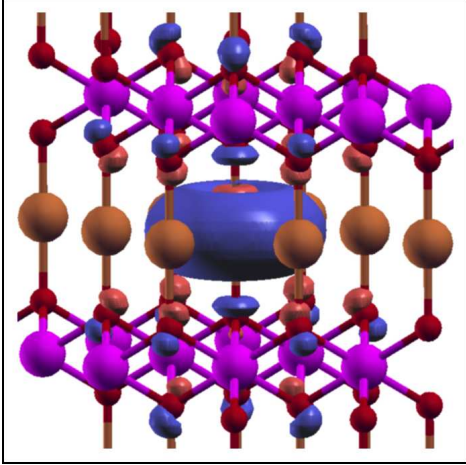


Fig. 5: (Color online.) Isosurface of the Wannier function for the Cu  $d_{z^2}$  orbital in the  $x=0.3$  doped metal. Antibonding contributions are seen from the nearest O atoms (small red spheres). The metallic state contains contributions from O ions in the second layer above and below that are not present in the insulator.

O atoms between Cu layers, it is the source of the increase in  $t_{\perp}$  hopping seen in Table 1 that leads to the  $k_z$  dispersion of the  $2p$  band along L-U in Fig. 4 (and more so along  $\Gamma$ -T, not shown), and will promote good hole-conduction in hole-doped delafossites.

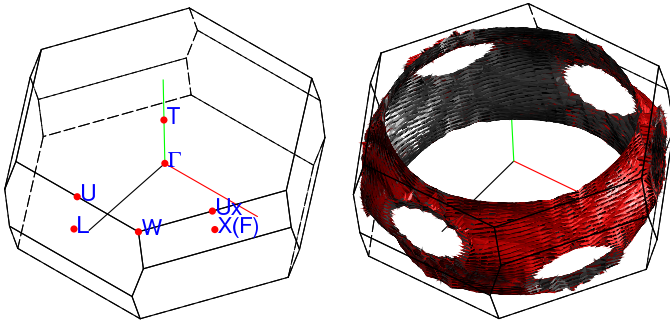


Fig. 6: (color online) Left: rhombohedral zone with special k-points labeled. Right: the sole large multiply-connected Fermi surface for moderately hole doped  $\text{CuAl}_{1-x}\text{Mg}_x\text{O}_2$ ,  $x = 0.3$ .

Fermi surfaces (FS) are critical to a material once it is doped into a metallic phase. For small hole doping, the FS lies close to the zone boundary everywhere. The FS of  $\text{CuAlO}_2$  for  $x = 0.3$  hole doping in VCA, displayed in Fig. 6(b), is not so different from that shown by NK for rigid band doping, but the self-consistent treatment will differ substantially, for larger doping levels, with new sheets appearing due to the spectral weight transfer. The FS resembles a somewhat bloated cylinder truncated by the faces of the rhombohedral BZ. The relevant nesting, not necessarily strong, is of two types. A large  $2k_F$  spanning wavevector almost equal to the BZ dimension in the  $k_x - k_y$  plane will, when reduced to the first BZ, lead to

small  $q$  scattering on the FS, broadened somewhat by the  $k_z$  dispersion. Second, there are “skipping”  $\vec{q}$  values along  $(\epsilon, \epsilon, q_z)$  for small  $\epsilon$ . It is for these values of  $\vec{q}$  that NK reported extremely strong coupling. We have focused our study of EPC on the regime  $x \sim 0.3$  of doping where NK predicted the very large electron-phonon coupling and high  $T_c$ .

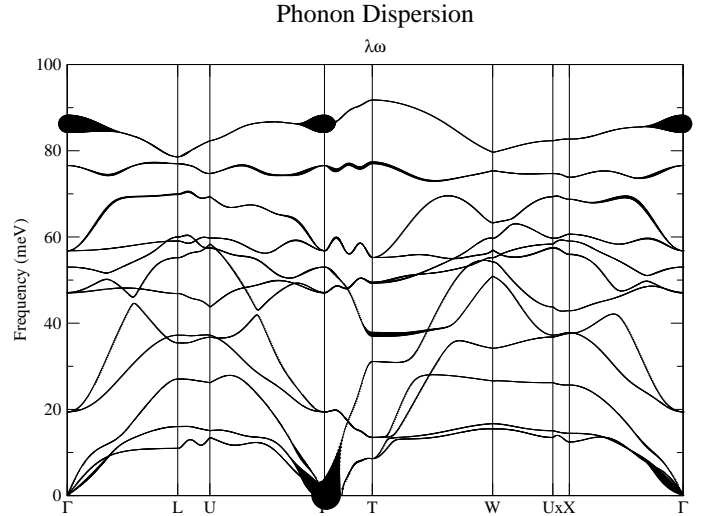


Fig. 7: Phonon dispersion curves for  $x=0.3$  hole-doped  $\text{CuAlO}_2$ , calculated with the ABINIT code on a  $8^3$   $q$ -point grid with  $24^3$  k-points. Circles indicate the magnitude of  $\lambda_q \omega_q$  for that mode. Some aliasing effects (unphysical wiggles) along L-U and  $\Gamma$ -T are due to the discrete nature and orientation of the  $q$ -point mesh.

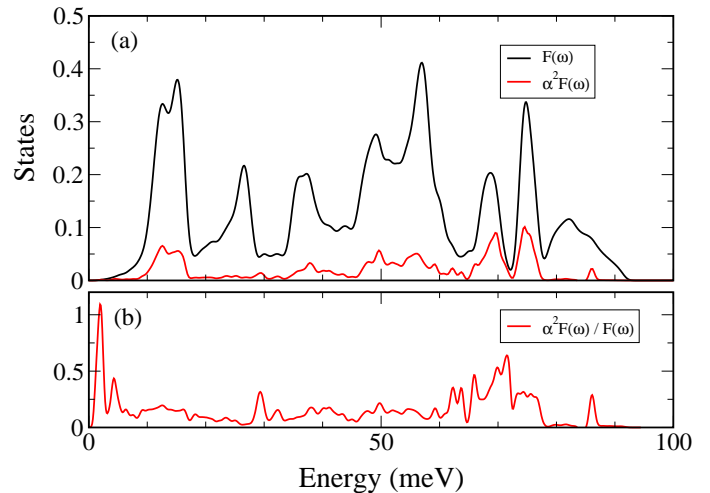


Fig. 8: (a) The phonon density of states and  $\alpha^2 F(\omega)$  at  $x = 0.3$ . (b) The quotient  $\alpha^2(\omega) = \alpha^2 F(\omega) / F(\omega)$  reflecting the spectral distribution of the coupling strength. The peaks below 5 meV are numerically uncertain and are useless for EPC due to the vanishingly small density of states.

To assess the effects of the spectral shifts, we have computed the phonons and electron-phonon using linear response theory. The phonon dispersion curves calculated from DFT linear response theory at  $x = 0.3$  are presented in Fig. 7, with

fatbands weighting by  $\omega_q \lambda_q$  (which is more representative of contribution to  $T_c$  than by weighting by the “mode- $\lambda$ ”  $\lambda_q$  alone [32]). Branches are spread fairly uniformly over the 0-90 meV region. As found by NK, coupling strength is confined to the Cu-O stretch mode at 87 meV very near  $\Gamma$ , and to very low frequency acoustic modes also near  $\Gamma$  where the density of states is very small. Unlike in  $\text{MgB}_2$ , this coupling does *not* extend far along  $k_z$ ; the lack of strong electronic two-dimensionality degrades EPC coupling strength greatly and no modes show significant renormalization. We obtain  $\lambda \approx 0.2$ ,  $\omega_{log}=275\text{K} = 24$  meV. Using the weak coupling expression with  $\mu^* \sim 0.1$  we obtain

$$T_c \approx \frac{\omega_{log}}{1.2} e^{-\frac{1}{\lambda-\mu^*}} \sim 230 e^{-10} K, \quad (1)$$

so no observable superconductivity is expected.

Similar to that obtained by NK, the largest electron-phonon coupling arises from the O-Cu-O bond stretch mode. As anticipated from the FS shape, the most prominent contributions arise from small  $q$  phonons. The EPC spectral function  $\alpha^2 F(\omega)$  is compared in Fig. 8(a) with the phonon DOS  $F(\omega)$ . As is apparent from their ratio shown in Fig. 8b, the peak around 15 meV is purely from the large density of states there, due to the flat phonon bands over much of the zone at that energy. The coupling with much impact on  $T_c$  (*i.e.* area under  $\alpha^2 F$ ) occurs in the 45-75 meV range, and is spread around the zone; however, unlike  $\text{MgB}_2$  no frequency range is dominant and the coupling is weak. The top O-Cu-O stretch mode, with the largest  $\lambda$  values and in the 80-90 meV range, are so strongly confined to narrow  $q$  ranges that they contribute little to the coupling.

While we conclude, morosely, that high  $T_c$  EPC superconductivity will not occur in doped  $\text{CuAlO}_2$ , the behavior that has been uncovered provides important insight into materials properties design beginning from 2D insulators. In the 40K electron-phonon superconductor  $\text{MgB}_2$  superconductor, an interlayer charge transfer of much smaller magnitude and natural origin self-dopes the boron honeycomb sublattice to become the premier electron-phonon superconductor of the day. Hole doping of this delafossite does not provide better superconductivity, but it does provide insight into designing materials behavior as well as providing a new platform for complex electronic behavior. For low concentrations small polaron transport has been observed. [29] The hole-doping spectral shifts are distinct from doping-induced spectral shifts in Mott insulators, which typically occurs without charge transfer. As for the envisioned behavior: at moderate doping this materials class provides a single band (Cu  $d_{z^2}$ ) triangular lattice system, with  $\text{Cu}^{2+}$   $S=1/2$  holes, which if coupling is antiferromagnetic leads to frustrated magnetism. The unusual dispersion at low doping, with little dispersion along  $k_z$  and also around the zone boundary, leads to an effectively *one dimensional phase space* at the band edge, although this property degrades rapidly with doping. Another triangular single band transition metal compound [33, 34] is  $\text{LiNbO}_2$ , which superconducts around 5K when heavily hole doped [33] and whose mechanism of pairing remains undecided.

This work was supported by DOE SciDAC grant DE-FC02-06ER25794 and a collaborative effort with the Energy Frontier Research Center *Center for Emergent Superconductivity* through SciDAC-e grant DE-FC02-06ER25777. W.E.P. acknowledges the hospitality of the Graphene Research Center at the National University of Singapore where this manuscript was completed.

## REFERENCES

- [1] W. E. Pickett, Physica B **296**, 112 (2001) provides an overview of such classes of superconductors.
- [2] W. E. Pickett, D. J. Singh, D. A. Papaconstantopoulos, H. Krakauer, M. Cyrot, and F. Cyrot-Lackmann, Physics C **162-164**, 1433 (1989).
- [3] R. Viennois, E. Giannini, J. Teyssier, J. Elia, J. Deisenhofer, and D. van der Marel, J. Phys.: Conf. Ser. **200**, 012219 (2010).
- [4] R. Arita, A. Yamasaki, K. Held, J. Matsuno, and K. Kuroki, J. Phys.: Cond. Matt. **19**, 365204 (2007).
- [5] D. Kasinathan, A. B. Kyker, and D. J. Singh, Phys. Rev. B **73**, 214420 (2006).
- [6] J. Chaloupka and G. Khaliullin, Phys. Rev. Lett. **100**, 016404 (2010).
- [7] S. Kouno, N. Shirakawa, Y. Yoshida, N. Umeyama, K. Tokiwa, and T. Watanabe, J. Phys.: Cond. Matt. **21**, 285601 (2009).
- [8] E. Benckiser, M. W. Haverkort, S. Brück, E. Goering, S. Macke, A. Frano, *et al.*, Nat. Matl. **10**, 189 (2011).
- [9] N. A. Spaldin and W. E. Pickett, J. Solid State Chem. **176**, 615 (2003).
- [10] K. Le Hur, C.-H. Chung, and I. Paul, Phys. Rev. B **84**, 024526 (2011).
- [11] E. Coronado, C. Marti-Gastaldo, E. Navarro-Moratalla, A. Ribera, S. J. Blundell, and P. J. Baker, Nature Chem. **2**, 1031 (2010).
- [12] V. Pardo and W. E. Pickett, Phys. Rev. B **80**, 054415 (2009).
- [13] H. Katayama-Yoshida, K. Kusakabe, H. Kizaki, and A. Nakanishi, Appl. Phys. Exp. **1**, 081703 (2008).
- [14] D. J. Scalapino, J. R. Schrieffer, and J. W. Wilkins, Phys. Rev. **148**, 263 (1966).
- [15] W. E. Pickett, J. Supercond. Novel Magn. **19**, 291 (2006).
- [16] A. Nakanishi and H. Katayama-Yoshida, Solid State Commun. **152**, 24 (2012); *ibid.* **152**, 2078 (2012).
- [17] J. An and W. E. Pickett, Phys. Rev. Lett. **86**, 4366 (2001).
- [18] Y. Kong, O. V. Dolgov, O. Jepsen, and O. K. Andersen, Phys. Rev. B **64**, 020501 (2001).
- [19] J. Kortus, I. I. Mazin, K. D. Belashchenko, V. P. Antropov, and L. L. Boyer, Phys. Rev. Lett. **86**, 4656 (2001).
- [20] K.-P. Bohnen, R. Heid, and B. Renker, Phys. Rev. Lett. **86**, 5771 (2001).
- [21] H. Kawazoe, M. Yasukawa, H. Hyodo, M. Kurita, H. Yanagi, and H. Hosono, Nature **389**, 939 (1997).
- [22] G. Dong, M. Zhang, W. Lan, P. Dong, and Y. Yan, Vacuum **82**, 1321 (2008).
- [23] W. E. Pickett, Phys. Rev. Lett. **73**, 1664 (1994).
- [24] K. M. O'Donnell, T. L. Martin, N. A. Fox, and D. Cherno, Phys. Rev. B **82**, 115303 (2010).
- [25] K. Koepf and H. Eschrig, Phys. Rev. B **59**, 1743 (1999).
- [26] X. Gonze, J.-M. Beuken, R. Caracas, F. Detraux, M. Fuchs, G.-M. Rignanese, L. Sindic, M. Verstraete, G. Zerah, F. Jollet, *et al.*, Comp. Mat. Sci. **25**, 478 (2002).

- [27] J. P. Perdew and Y. Wang, Phys. Rev. B **45**, 13244 (1992).
- [28] B. U. Koehler and M. Jansen, Z. Anorg. Allg. Chem. **543**, 73 (1986).
- [29] B. J. Ingram, T. O. Mason, R. Asahi, K. T. Park, and A. J. Freeman, Phys. Rev. B **64**, 155114 (2001).
- [30] H. Yanagi, S.-I. Inoue, K. Ueda, H. Kawazoe, H. Hosono, and N. Hamada, J. Appl. Phys. **88**, 459 (2000).
- [31] W. Ku, H. Rosner, W. E. Pickett, and R. T. Scalettar, Phys. Rev. Lett. **89**, 167204 (2002).
- [32] P. B. Allen, Phys. Rev. B **6**, 2577 (1972).
- [33] M. J. Geselbracht, T. J. Richardson, and A. M. Stacy, Nature (London) **345**, 324 (1990).
- [34] E. R. Ylvisaker and W. E. Pickett, Phys. Rev. B **74**, 075104 (2006).

		Insulator			Metal		
		$z^2$	$xy$	$x^2 - y^2$	$z^2$	$xy$	$x^2 - y^2$
$z^2$	$t_1$	<b>393</b>	198	228	<b>342</b>	191	220
	$t_2$	60	8	13	60	14	17
	$t_3$	<b>35</b>	22	25	<b>59</b>	17	20
	$t_\perp$	<b>24</b>	15	-16	<b>63</b>	17	17
$xy$	$t_1$		123	117		107	107
	$t_2$		35	14		36	16
	$t_3$		11	8		11	10
	$t_\perp$		23	14		31	20
$x^2 - y^2$	$t_1$			147			140
	$t_2$			28			27
	$t_3$			15			17
	$t_\perp$			18			23

Table 1: Tight binding hopping parameters for insulating and metallic phases, from the three constructed Wannier functions. The labels  $t_1$ ,  $t_2$ ,  $t_3$ , refer to the first, second, and third neighbor hoppings in the triangular Cu planes.  $t_\perp$  refers to hopping between layers. The most significant changes when doped are highlighted in bold print.